Immobilized dye-decolorizing peroxidase (DyP) and directed evolution variants for hydrogen peroxide biosensing

Catarina Barbosa [a,1], Célia M. Silveira [a,1], Diogo Silva [a], Vânia Brissos [a], Peter Hildebrandt [b], Lígia O. Martins [a,**], Smilja Todorovic [a,*]

[a] *Instituto de Tecnologia Química e Biológica António Xavier, Universidade NOVA de Lisboa, Av. da República, 2780-157, Oeiras, Portugal*
[b] *Technische Universität Berlin, Inbstitut für Chemie, Sekr. PC14, Straße des 17. Juni 135, D-10623, Berlin, Germany*

A B S T R A C T

Immobilized dye-decolorizing peroxidase from *Pseudomonas putida* MET94 (PpDyP) and three variants generated by directed evolution (DE) are studied aiming at the design of a biosensor for H_2O_2 detection. Structural properties of the enzymes in solution and immobilized state are addressed by resonance Raman (RR) and surface enhanced RR (SERR) spectroscopy, and the electrocatalytic properties are analyzed by electrochemistry. The wild-type (wt) and 29E4 variant (with E188K and H125Y mutations) represent excellent candidates for development of H_2O_2 biosensors, since they exhibit a good dynamic response range (1–200 μM H_2O_2), short response times (2 s) and a superior sensitivity (1.3–1.4 A·M^{-1}·cm^{-2}) for H_2O_2, as well as selectivity and long term stability. In contrast to the solution state, 6E10 (with E188K, A142V and H125Y mutations) and 25F6 (with E188K, A142V, H125Y and G129D mutations) variants display much lower activity and are inhibited by high concentrations of H_2O_2 upon adsorption on an electrode. In terms of sensitivity, the bioelectrodes employing wt PpDyP and 29E4 variant outperform HRP based counterparts reported in the literature by 1–4 orders of magnitude. We propose the development of wt or 29E4 PpDyP based biosensor as a valuable alternative to devices that rely on peroxidases.

1. Introduction

Mediatorless 3rd generation biosensors rely on direct electron transfer (DET) between an immobilized enzyme and an electrode, allowing for a sensitive detection of the enzyme's substrate (Bollella and Gorton, 2018; Das et al., 2016). In this respect, peroxidases represent an obvious choice for the design of H_2O_2 biosensors. Detection and quantification of H_2O_2 is highly relevant in pharmaceutical, textile, paper, food and chemical industries, where it is used as oxidant for whitening or sterilizing purposes (Zhang and Chen, 2017) as well as in medicine, as it plays roles of oxidative stress marker in aging and disease and of defense agent in response to pathogen invasion (Lippert et al., 2011). The reported values of H_2O_2 in biological samples cover a broad range of concentrations (μM-mM) (Forman et al., 2016), demanding for improved and more accurate methods for its detection that are at the same time less susceptible to interfering agents. Among peroxidases,

bacterial dye-decolorizing peroxidases (DyPs) reveal a particular potential, due to their broad substrate range, easy genetic manipulation to provide improved variants and high yields (Brissos et al., 2017; Colpa et al., 2014; Mendes et al., 2015a; Rahmanpour et al., 2016), and absence of glycosylation which interferes with DET (Presnova et al., 2000).

DyPs are relatively recently discovered enzymes that share no sequence homology and are structurally unrelated to classical heme peroxidases (Singh and Eltis, 2015; Sugano, 2009). DyPs lack the highly conserved distal histidine that acts as an acid-base catalyst in the catalytic reaction of classical peroxidases, which implies different mechanistic properties. Instead, they possess strictly conserved distal aspartic acid and arginine that can take up this role (Roberts et al., 2011; Singh et al., 2012; Sugano, 2009; van Bloois et al., 2010). The physiological function of DyPs is not fully established. Importantly, they are capable of efficient oxidation of structurally diverse substrates, including synthetic

dyes, metals, aromatic sulphides and phenolic and nonphenolic lignin units (Colpa et al., 2014; Mendes et al., 2015b; Santos et al., 2014; Sugano, 2009). These bulky substrates bind at the enzyme surface or nearby but outside of the heme pocket. In the case of the former the electrons that are used for the reduction of H_2O_2, travel to the ferric (Fe^{3+}) heme via long-range electron transfer routes that include surface-exposed tryptophanyl or tyrosyl radicals, similar to lignin (LiP) and versatile (VP) peroxidases (Linde et al., 2015). Systematic studies of peroxidases, and in particular resonance Raman (RR) spectroscopy, established that five-coordinated high-spin (5cHS) and six-coordinated high-spin (6cHS) heme species commonly co-exist in the resting states of bacterial and plant peroxidases, e.g. cytochrome c peroxidase (CCP), horse radish peroxidase (HRP), soy bean peroxidase (SBP), etc (Smulevich et al., 2005). The unusual quantum spin admixture (5cQS) species, present in e.g. KatG catalase peroxidase (Kapetanaki et al., 2003), was also identified in some DyPs and shown to be capable of H_2O_2 binding and reduction (Sezer et al. 2012a, 2013; Todorovic et al., 2015).

Active site structure of immobilized heme enzymes, which is relevant for the 3rd generation bio-electronic devices, often differs from that in solution due to immobilization-induced structural alterations, which inevitably also alter the catalytic properties of the enzyme (Todorovic et al., 2006). To that end, surface enhanced RR (SERR) spectroscopy sensitively probes the spin and oxidation state, and axial coordination pattern of the heme cofactor of enzymes immobilized on biocompatible plasmonic silver (Ag) supports. The metal that provides the surface enhancements of RR signals of the immobilized enzyme (giving origin to SERR) can furthermore serve as an electrode, allowing for monitoring the enzyme structure in an electrochemical setup (Ly et al., 2011; Murgida and Hildebrandt, 2001, 2004; Sezer et al., 2012b).

We have previously demonstrated that wild-type (wt) PpDyP, unlike DyPs from other sources, can be immobilized on biocompatible Ag electrodes under conditions in which the enzyme i) retains structural integrity, ii) reveals efficient DET with the electrode and iii) exhibits electrocatalytic H_2O_2 reduction (Sezer et al., 2012a). These are actually the main issues that impede faster advancement of construction of the 3rd generation biosensors in general (Bollella and Gorton, 2018), despite the many advantages that they offer, such as selectivity and a simplified electrochemical reaction scheme due to the lack of additional reagents. Here we explore in detail wt PpDyP and its variants that show improved catalytic properties and stability, as biocatalysts for development of electrochemical H_2O_2 biosensors. The variants are obtained by directed evolution (DE), which represents the most efficient method for tailoring PpDyP for desired properties (Brissos et al., 2017). We successively apply several levels of criteria to discriminate among the biocatalysts based on their structure and catalytic performance in solution and immobilized states, and identify the best candidate for construction of the 3rd generation PpDyP based H_2O_2 biosensor.

2. Experimental

2.1. Enzyme expression and purification

Cloning, overexpression and purification of wt and evolved variant PpDyPs was performed in *E. coli* following previously optimized procedures (Brissos et al., 2017; Santos et al., 2014). The DE variants were generated by random mutagenesis using error prone PCR. Screening and selection of evolved variants was performed in 96-well plates; the activity of crude extracts was determined in the presence of 2,6-dimethoxyphenol (DMP). The variant with the highest stability was chosen to be the parent for the next generation, namely 6E10 → 29E4 → 25F6 (cf. detailed experimental information regarding the cloning, expression and purification of PpDyP variants in Supplementary Material).

2.2. Apparent steady-state kinetic analysis

Enzymatic activities of wt and variant PpDyPs were monitored using either a Nicolet Evolution 300 spectrophotometer from Thermo Industries (Madison, USA) or a Synergy2 microplate reader (BioTek, Vermont, USA) at 25 °C. The optimal pH (pH_{opt}) was determined by monitoring the oxidation of 3 mM 2,2′-azino bis (3-ethylbenzthiazoline-6-sulfonic acid) (ABTS) at 420 nm in the presence of 1 mM H_2O_2 at 25 °C using Britton-Robinson buffer (100 mM phosphoric acid, 100 mM boric acid, and 100 mM acetic acid mixed with NaOH to the desired pH in the range 2–11). The kinetic parameters for H_2O_2 (0.005–5 mM) were measured in the presence of 3 mM ABTS ($\varepsilon_{420nm} = 36,000$ $M^{-1}cm^{-1}$) in 100 mM sodium acetate, at the pH_{opt} of the enzyme (Brissos et al., 2017). Kinetic data was fitted directly using the Michaelis-Menten equation or the equation for non-linear curve that fits enzyme kinetics affected by substrate inhibition ($v = V_{max}[S]/(K_M+[S](1+[S]/K_i))$) (Origin software).

2.3. Enzyme stability assays

Thermal inactivation assays were performed as previously described (Santos et al., 2014). In brief, enzyme solutions were incubated at 60 °C in 20 mM Tris-HCl buffer, pH 7.6, and at fixed time intervals, sample aliquots were withdrawn and tested for activity following DMP oxidation (at 468 nm) at 25 °C. Residual activities (A_t/A_0, where A_t is the activity measured at time t and A_0 is the initial activity at $t = 0$) were plotted versus the incubation time. Inactivation constants k_{in} were obtained by linear regression of (ln activity) versus t. The half-life value of thermal inactivation $t_{1/2}$ was calculated using $t_{1/2} = \ln2/k_{in}$.

2.4. Bioelectrode preparation

The Ag ring electrodes (geometrical area 0.7 ± 0.05 cm^2) were prepared as described previously (Murgida and Hildebrandt, 2001; Sezer et al., 2012a; Wackerbarth et al., 1999). In brief, the SERR-active Ag electrodes were incubated overnight in SAM solution, containing 1 mM amino-octanethiol (AOT) and 3 mM mercapto-hexanol (MOH) in ethanol. Gold electrodes (Au) (∅ 2 mm, BASi) were polished in 1, 0.3 and 0.05 μm (Buehler) alumina slurry, sonicated in deionized water and incubated in SAM solution overnight (vide supra). The SAM coated electrodes were then rinsed with buffer and immersed into a solution containing 0.2 μM enzyme (in 12.5 mM potassium phosphate buffer solution at pH 7.0, with 12.5 mM K_2SO_4) for 30 min, prior to measurements. For stability assays, the electrodes were stored in buffer at 4 °C.

2.5. Spectroscopy

RR and SERR spectra were acquired with Raman spectrometer (Jobin Yvon LabRam 800 HR) with a back-illuminated CCD detector cooled by liquid nitrogen; an Olympus 20× objective was used for laser focusing onto the sample and light collection in the backscattering geometry. The 413 nm line from a Krypton ion laser (Coherent Innova 300c) was used as the excitation source. The RR spectra of 100–200 μM enzyme were measured in a rotating cuvette (Hellma). The potential-dependent SERR experiments were performed using a home-built spectroelectrochemical cell equipped with a three-electrode arrangement: the SAM/enzyme modified Ag working electrode, an Ag/AgCl (3 M, KCl) reference electrode (WPI) and a platinum wire counter electrode (Goodfellow). Electrode potentials were controlled using a Princeton Applied Research 263A potentiostat. The experiments were carried out in supporting electrolyte (12.5 mM potassium phosphate buffer solution at pH 7.0, containing 12.5 mM K_2SO_4). The working electrode was kept under constant rotation (3000 rpm) to prevent prolonged exposure of individual enzyme molecules to laser irradiation. The laser power was 3 mW and accumulation times were 30 and 20 s in SERR and RR experiments, respectively; typically 4–10 spectra were co-added in each measurement to improve signal to noise (S/N) ratio.

Table 1
Kinetic and analytical characterization of wt PpDyP and variants in solution and immobilized state. Apparent steady-state kinetic parameters for reduction of H_2O_2 were determined in solution using ABTS as reducing substrate at 25 °C and at the pH_{opt} of the enzymes. The response of PpDyP/SAM/Ag electrodes to H_2O_2 was determined at RT and pH 7.0. Limit of detection (LOD) was determined at S/N of 3. Reproducibility is represented as the variation of catalytic current at 50 μM H_2O_2 for different electrode preparations (n = 6–8). nd - not detected; * - taken from (Santos et al., 2014).

	PpDyP	wt	6E10	29E4	25F6
	mutations	–	E188K/A142V/H125Y	E188K/H125Y	E188K/A142V/H125Y/G129D
solution	pH	4.3*	5.5	4.5	5.5
	K_M^{app} (μM)	60 ± 10*	57 ± 18	87 ± 11	268 ± 23
	k_{cat} (s^{-1})	23 ± 2*	13 ± 2	43 ± 1	9 ± 1
	k_{cat}/K_M (M^{-1}·s^{-1})	$(4 ± 1) \times 10^5$*	$(2 ± 1) \times 10^5$	$(5 ± 1) \times 10^5$	$(3 ± 1) \times 10^4$
	K_i (mM)	0.7 ± 0.1*	nd	0.9 ± 0.1	nd
immobilized	pH	7.0	7.0	7.0	7.0
	K_M^{app} (mM)	0.43 ± 0.02	0.18 ± 0.01	0.22 ± 0.03	0.14 ± 0.03
	J_{max} (μA·cm^{-2})	−832 ± 19	−222 ± 6	−550 ± 23	−65 ± 7
	K_i (mM)	nd	3.5 ± 0.3	nd	1.1 ± 0.2
	Linear Range (μM)	1–200	1–50	1–150	1–50
	LOD (μM)	3.6	1.5	3.2	3.6
	Sensitivity (A·M^{-1}·cm^{-2})	1.31 ± 0.03	0.98 ± 0.02	1.38 ± 0.03	0.35 ± 0.02
	Reproducibility	97%	86%	96%	89%

2.6. Electrochemistry

The bioelectrodes were characterized at room temperature (RT) by cyclic voltammetry (CV) and chronoamperometry, performed in the SERR spectroelectrochemical cell (cf. above). Prior to measurements, the supporting electrolyte (10 mL) was deoxygenated by bubbling argon for 20 min; the cell was maintained under argon atmosphere during the course of the experiment. Cyclic voltammograms were recorded in the range of 0.3 to −0.15 V at a scan rate of 50 mV·s^{-1}. The chronoamperograms (I vs. t) were performed at an applied potential of 0.1 V and under a rotation speed of 2600 rpm. Response of the bioelectrode to H_2O_2 was evaluated by successive injections of previously deoxygenated stock solutions to the cell. The catalytic currents (I_{cat}) were corrected by subtracting the current measured in the absence of substrate. Concentration of H_2O_2 in stock solutions was determined spectrophotometrically using a molar absorption coefficient of 43.6 M^{-1}·cm^{-1} at 240 nm (Hildebrandt and Roots, 1975). Kinetic data were fitted either with the electrochemical Michaelis-Menten equation or Michaelis-Menten affected by substrate inhibition ($I_{cat} = I_{max}$ [S]/(K_M + [S]/(1 + [S]/K_S))). All potentials are quoted vs. the normal hydrogen electrode (NHE) (+0.205 V vs. Ag/AgCl, 3 M KCl).
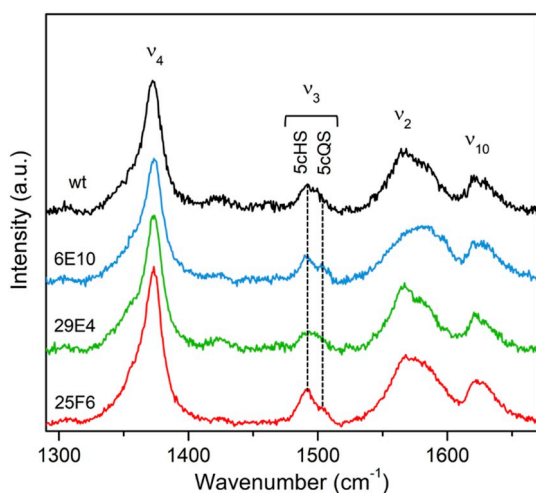
Fig. 1. High frequency region of SERR spectra of wt, 6E10, 29E4 and 25F6 PpDyPs attached to SAM coated Ag electrodes. Measurements were performed at open circuit potential (ca. 0.29 V). Spectra were acquired with 413 nm excitation at RT, with 3 mW laser power and 30 s accumulation time.

3. Results and discussion

3.1. Directed evolution PpDyP variants with improved properties

The 6E10 PpDyP variant, evolved after three rounds of DE, exhibits a 100-fold improved catalytic efficiency for phenolic substrate DMP and resistance to H_2O_2 inactivation but nevertheless limited thermo-stability (Brissos et al., 2017). It harbors three mutations (E188K, A142V and H125Y) at the surface of the enzyme, in the second shell of the heme cavity. Using 6E10 as parent, the 29E4 variant showing ~ 5-fold higher thermo-stability, was identified among ~4000 clones. Its sequence reveals the loss of A142V mutation present in 6E10 (Fig. S1). In the following round of DE, using 29E4 as parent, a hit 25F6 was identified, showing 1.7-fold higher thermo-stability than 29E4. It carries A142V and G129D mutations (Fig. S1). The catalytic properties of the purified variants, determined at the respective pH_{opt} for H_2O_2 substrate, reveal that elimination of the A142V in 29E4 variant results in a catalytic efficiency (k_{cat}/K_M) similar to that of 6E10. A reintroduction of this mutation, together with the G129D, in 25F6 variant results in one order of magnitude lower k_{cat}/K_M (Table 1) (Brissos et al., 2017). The thermal inactivation profiles, obtained from kinetic stability assays performed at 60 °C, indicate that 29E4 and 25F6 variants have a higher half-life inactivation (43 ± 11 min^{-1} and 36 ± 9 min^{-1}, respectively) than 6E10 and wt (7 ± 1 min^{-1} and 15 ± 2 min^{-1} respectively) (Fig. S2).

3.2. Immobilized PpDyPs

Wt PpDyP and variants were electronically coupled to biocompatible AOT/MOH (1:3) coated metal electrodes and evaluated as platforms for development of the 3rd generation biosensors. The active site structures of the immobilized enzymes were probed by SERR spectroscopy. The comparison of RR spectra of the enzymes in solution and the respective SERR spectra measured upon immobilization on modified nano-structured Ag electrodes allow for the detection of the eventual immobilization-induced structural changes (Ly et al., 2011; Murgida and Hildebrandt, 2004; Sezer et al., 2012b; Todorovic et al. 2006, 2008). The high frequency region of SERR spectra of the wt and variant PpDyPs reveals the presence of multiple heme sub-states (Figs. 1 and S3b). Two major heme species co-exist in the spectra of the 6E10, 29E4 and 25F6 variants, which we attribute to 5-coordinated high-spin (5cHS) and 5-coordinated quantum mechanically mixed-spin (5cQS) species (Sezer et al. 2012a, 2013). This is particularly evident from the analysis of the v_3 marker band, sensitive to heme coordination and spin states, that displays two bands centered at 1491 and 1500 cm^{-1}, originating from 5cHS and 5cQS respectively, Fig. 1.

A comparison of RR with SERR spectra indicates no major alterations of the oxidation or coordination state of the heme or appearance of new bands in the SERR spectra, Fig. S3a. A deconvolution of SERR spectra reveals a presence of the same heme species detected in RR spectra, but with altered relative abundance, Fig. S3b and Table S1; the 5cHS state becomes dominant in the immobilized enzymes. We observe approx. 3 cm^{-1} upshift of ν_3(5cQS) modes in SERR spectra of 6E10 and 25F6 PpDyPs, which in the case of some heme proteins could be indicative of formation of 6cLS population. Nevertheless, the ν_3(6cLS) is in DyPs expected at much higher frequencies (Sezer et al. 2012a, 2013). We attribute these findings to different selection rules for RR and SERR effects and/or possibly non-uniform orientation of the attached enzyme to the electrode (Bernad et al., 2004; Kanger and Otto, 2003; Todorovic et al., 2012). It is noteworthy that the mutations do not affect the enzyme's active site structure, since the same spin populations, with the similar relative abundance are observed in RR spectra of the wt PpDyP and variants (Fig. S3a, lower traces, and Table S1). This can be rationalized in terms of the relative positions and the nature of the amino acid substitutions (Brissos et al., 2017) (Fig. S1).

In the next step, we probed the redox behavior of PpDyPs attached to AOT/MOH coated Ag electrodes. The SERR spectra of the immobilized enzymes were measured at poised electrode potentials in 0.3 and −0.3 V interval (Fig. S4). The potential-dependent SERR spectra show that PpDyPs can be readily reduced or oxidized in the immobilized state, as indicated by the characteristic shifts of heme redox state sensitive marker bands (e.g. ν_4 and ν_3). The redox reaction is fully reversible (Fig. S4, traces a and h); the immobilized enzymes can withstand multiple redox cycles without apparent denaturation, revealing efficient and reversible heterogeneous ET. The SERR signal intensity nevertheless decreases after extended exposure of the enzymes to negative potentials, implying reduction- or potential-induced desorption of the enzymes, which must be taken into consideration in further applications. Altogether, we demonstrate that the active site architecture of PpDyP variants developed by DE does not differ from that of the wt. More importantly for the development of DyP based biosensors, the enzymes' active site structure remains intact upon immobilization. Therefore, we can conclude that at this point that wt PpDyP and all three evolved variants appear to be promising candidates for the development of DyP based sensors, as the respective active site structures and stability are preserved upon immobilization, and they exhibit efficient and reversible ET.

3.3. PpDyP-based bioelectrodes for electrochemical biosensor development

Once the preservation of the native structure of immobilized PpDyPs is ensured, as established by SERR spectroscopy, the electrocatalytic properties of PpDyP/SAM/Ag constructs were probed by CV. Upon addition of H_2O_2 to the SERR cell, the cathodic current increases due to the catalytic reduction by the enzymes attached to the working electrode, Fig. S5a. We attribute these catalytic currents to the formation compound I (i.e. catalytic intermediate $[Fe^{4+}=O]^{+\bullet}$) that is in PpDyP stabilized upon reaction of the ferric enzyme with H_2O_2, which is subsequently reduced by the electrode (Sezer et al., 2012a; Todorovic et al., 2015). Note that non-catalytic redox peaks could not be observed in the cyclic voltammograms, most likely due to insufficient amount of the enzyme on the electrode surface.

The choice of the electrode support. Both Ag and Au electrodes were tested. Ag substrates are required for surface enhancement of the RR signal (vide supra) in SERR experiments, but they have limited working potential window, defined by the oxidation of the Ag at 0.3 V and reductive desorption of the SAM below −0.34 V (Munakata et al., 2004). For that reason the negative current is already present at the start of the scan (0.3 V), Fig. S5a. Au electrodes allow for application of a wider potential window (up to 0.9 V). PpDyP/SAM/Au electrodes show a typical catalytic shape current–potential curve in the presence of

H_2O_2. The cathodic current peak at ca. 0.83 V (10 μM H_2O_2) shifts to lower values as the substrate concentration is increased, Fig. S5b. The catalytic current densities obtained at the PpDyP/SAM/Ag electrode are one order of magnitude higher than those measured with the Au counterparts; the modified Ag electrodes were therefore selected for further studies.

The choice of immobilized enzyme, wt vs. variants. The response of wt, 6E10, 29E4 or 25F6 electrodes to H_2O_2 was further characterized by chronoamperometry at a potential of 0.1 V, at which direct non-enzymatic reduction of H_2O_2 by the electrode is negligible; both Ag and Au electrodes show catalytic currents close to maximum at this potential, Fig. S5. The amperometric response recorded upon successive injections of deoxygenated stock solution of H_2O_2 to the cell (1 μM-2 mM final concentration) reveals the stepwise increase of the catalytic current at very short response times (<2 s), indicative of efficient heterogeneous ET (Fig. 2).

Control experiments performed with SAM/Ag electrodes without attached enzyme show a negligible increase of cathodic current upon addition of H_2O_2, about 0.2% of the current measured for wt PpDyP in the presence of 200 μM H_2O_2. The plots of catalytic current (I_{cat}) vs. substrate concentration, measured for all PpDyP/SAM/Ag electrode constructs show a distinct dependence for the studied enzymes, as depicted by electrochemical Michaelis–Menten equation fit to the data, Fig. 3a (Monteiro and Almeida, 2019).

The wt and 29E4 bioelectrodes reach a plateau for concentrations of H_2O_2 higher than 0.4 mM, which is indicative of a Michaelis-Menten-type enzyme kinetics (Fig. 3a, top two traces). The apparent Michaelis-Menten constant (K_M^{app}) and maximum current density at saturating substrate concentration (J_{max}) values are lower for the 29E4 (0.14 mM and −550 μA·cm^{-2}) than for the wt PpDyP (0.43 mM and −832 μA·cm^{-2}), Table 1, indicating a higher affinity for H_2O_2 but slightly lower activity of the immobilized 29E4. In solution, the analogous K_i and K_M values are 0.7 mM and 60 μM for wt PpDyP and 0.9 mM and 87 μM for 29E4, while k_{cat}/K_M are nearly identical (4 and 5 × 10^5 M^{-1}s^{-1}, respectively). This is consistent with substrate inhibited enzyme kinetics of wt and 29E4 PpDyPs in solution and slightly higher affinity of the former for H_2O_2. The catalytic currents of immobilized 6E10 and 25F6 are lower (−220 and −65 μA·cm^{-2}) and decrease with increasing H_2O_2 concentration (above 0.4 and 0.8 mM respectively). In solution, the 6E10 and 25F6 variants do not show substrate inhibition; the respective K_M and k_{cat}/K_M values are 57 μM and 2 × 10^5 M^{-1}s^{-1} for the former and 268 μM and 3 × 10^4 M^{-1}s^{-1} for the latter (Table 1). It appears that the decrease in electrocatalytic current can be related to the A142V mutation that both 6E10 and 25F6 carry. The absence of H_2O_2

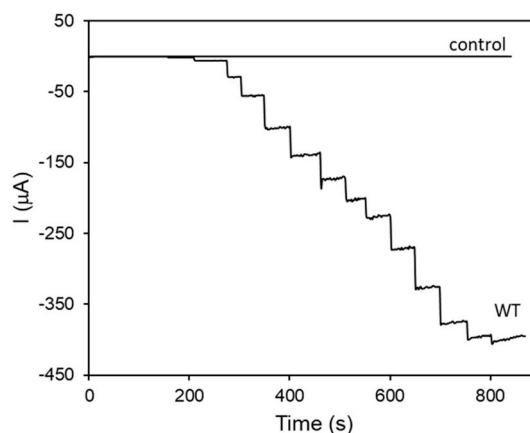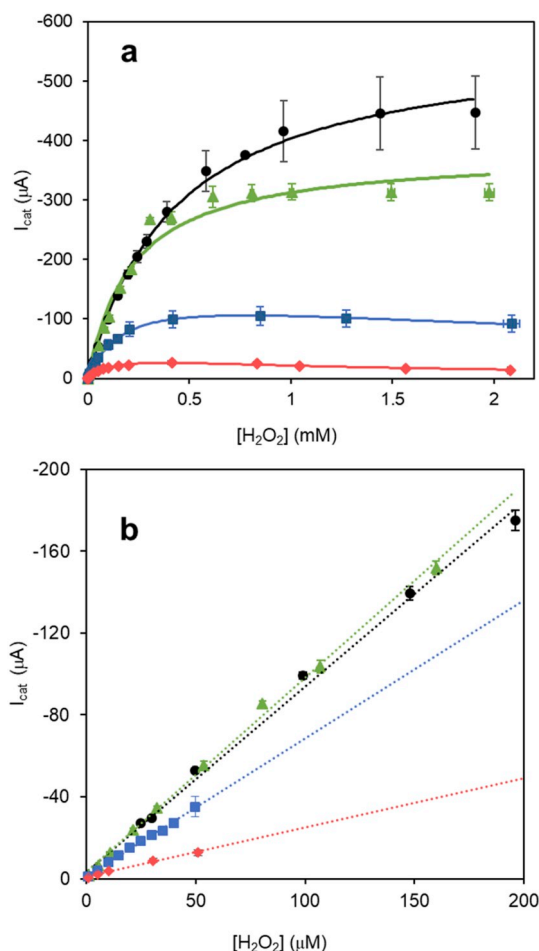**Fig. 2.** Amperometric response of SAM/Ag (control) and wt PpDyP/SAM/Ag electrodes to increasing concentrations of H_2O_2 (0.001–2 mM). Measurements performed in 12.5 mM K_2SO_4 in 12.5 mM PBS, pH 7.0, at applied potential of 0.1 V. The electrode was rotated at 2600 rpm to minimize the effect of substrate mass transport to the immobilized enzyme.

Fig. 3. a) Michaelis–Menten plots of catalytic currents vs. H_2O_2 concentration for wt (black circles), 6E10 (blue squares), 29E4 (green triangles) and 25F6 (red diamond) PpDyP/SAM/Ag electrodes. The relative standard deviations (RSD) vary between 2 and 6% for wt and 29E4 and 7–15% for 6E10 and 25F6 electrodes; wt displays ca. 15% RSD for $[H_2O_2] > 1$ mM; b) Linear dependence of the catalytic current on H_2O_2 concentration (n = 6–8), with slope and r^2 of 1.31 $A \cdot M^{-1} \cdot cm^{-2}$ and 0.996 (wt), 0.98 $A \cdot M^{-1} \cdot cm^{-2}$ and 0.996 (6E10), 1.38 $A \cdot M^{-1} \cdot cm^{-2}$ and 0.997 (29E4), and 0.35 $A \cdot M^{-1} \cdot cm^{-2}$ and 0.989 (25F6). (For interpretation of the references to color in this figure legend, the reader is referred to the Web version of this article.)

inhibition in the case of these two mutants in solution was rationalized in terms of conformational rearrangements in the heme cavity caused by A142V substitution, which leads to shielding of sensitive amino acids from H_2O_2 induced oxidation (Brissos et al., 2017). This behavior was not translated to the immobilized state, since the kinetic parameters of the single A142V variant are comparable to those of immobilized 6E10 and 25F6 (Fig. S6). An improved performance of wt and 29E4 PpDyPs is nevertheless clearly evident upon immobilization of these enzymes. The discrepancy between enzymes' behavior in solution and immobilized states can be tentatively attributed to the fact that the attachment of an enzyme to a solid electrode support alters its rotational freedom and may affect substrate accessibility. Furthermore, electrons for the catalytic reaction are provided by an electrode, and the ET pathways are most likely different than in solution, in which the apparent steady-state kinetic parameters for reduction of H_2O_2 are determined using ABTS as reducing substrate. An additional variable is pH; envisaging broad range of physiologically relevant applications, all measurements reported in this work were performed at pH 7, while the solution measurements refer to acidic pH_{opt} for each enzyme. It is noteworthy that the affinity for H_2O_2 of all four DyPs decreases in the immobilized state, as the K_M values are 2–5 times higher for the adsorbed enzymes than in solution

(Brissos et al., 2017; Mendes et al., 2015a; Sezer et al., 2012a). This behavior is commonly observed for enzymes immobilized on electrode surfaces, and is typically attributed to the limited diffusion of the substrate to the enzyme's active site (Monteiro and Almeida, 2019).

The response of the wt PpDyP bioelectrode to H_2O_2 is linear from 1 to 200 μM; in the case of 29E4 it is slightly lower, 1–150 μM. The sensitivity, determined by the slope of the calibration curve, and the limit of detection, estimated at S/N of three, are 1.31 $A \cdot M^{-1} \cdot cm^{-2}$ and 3.6 μM, respectively for wt PpDyP and similarly, 1.38 $A \cdot M^{-1} \cdot cm^{-2}$ and 3.2 μM for 29E4 bioelectrode, Table 1. The analytical performance of the 6E10 and 25F6 electrodes is poorer, as expected given their kinetic behavior in the immobilized state (vide supra). The sensor-to-sensor reproducibility, determined by measuring the catalytic current of 6–8 bioelectrodes in 50 μM H_2O_2, varies between 96 and 97% for the wt and 29E4 (cf. Table 1). The 6E10 and 25F6 bioelectrodes display higher current variations and lower reproducibility. Since these two variants are in addition prone to substrate inhibition, we can conclude that they are not appropriate for biosensor development.

A number of features of the wt and 29E4 bioelectrodes are actually remarkable in comparison with examples found in the literature. The immobilized wt and 29E4 PpDyPs perform better than HRP, which was particularly explored for H_2O_2 biosensor construction, and which is used in the only commercially available H_2O_2 biosensing device. Wt and 29E4 PpDyP constructs show shorter response time and superior sensitivity in respect to the published enzyme based H_2O_2 biosensors, including those that employ nanomaterials that usually display high activities owing to increased loading of enzymes (Table 2). We show that both wt and 29E4 PpDyP have 1.3–1.4 $A \cdot M^{-1} \cdot cm^{-2}$ sensitivity, which is one to four orders of magnitude higher than the values reported in the literature for HRP based bioelectrodes, none of which exceeds 0.6 $A \cdot M^{-1} \cdot cm^{-2}$. The response time of 2 s is also shorter than in any of the reported HRP based systems. In terms of LOD, wt and 29E4 PpDyP bioelectrodes show an average behavior (3.6 μM) as it falls in the middle of 0.02–86 μM range reported for HRP based electrodes (Table 2). Their linear range is on the narrower side (1–200 and 1–150 μM for wt and 29E4 PpDyPs, respectively), while some HRP based systems span over concentrations of 3 orders of magnitude. This is nevertheless not necessarily a drawback as long as it is contemplated in the envisaged applications (vide supra). Taken together, we can conclude that wt PpDyP and 29E4 variant represent promising candidates for the construction of H_2O_2 biosensors and they were further tested (vide infra).
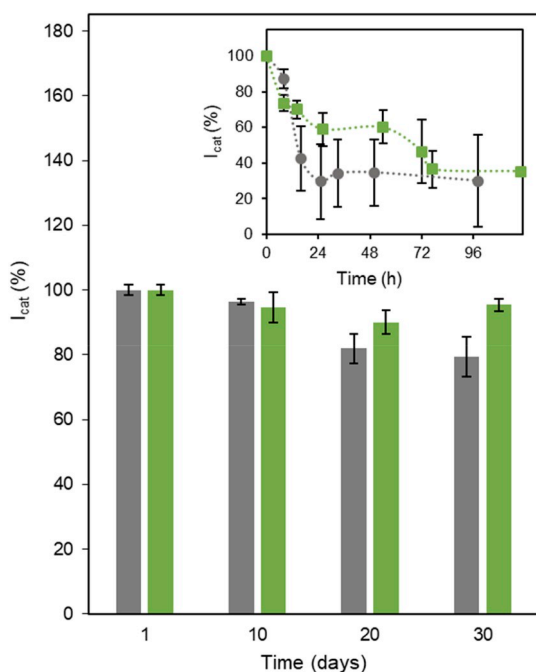
Stability of wt and 29E4 PpDyP bioelectrodes. The response stability of the wt and 29E4 PpDyP bioelectrodes was evaluated by measuring catalytic currents in the presence of 50 μM H_2O_2 in regular time intervals during one month period, using electrodes stored at 4 °C in supporting electrolyte. SERR spectra of stored electrodes reveal no significant changes at the level of enzyme's active site in comparison to that of the freshly immobilized enzyme (i.e. electrode prepared and measured on the same day) (Fig. S7). The shelf-life was evaluated by comparing sets of wt and 29E4 PpDyP bioelectrodes prepared on the same day. Both enzymes retain about 85–95% of the initial biocatalytic response (measured on day 1) during one month, Fig. 4. However, multiple uses of the same electrode causes an abrupt decrease of the initial activity (Fig. 4 inset), with estimated half-life of 13 h for wt and 36 h for 29E4. This could be due to enzyme desorption from the electrode (e.g. washing procedures, application of electrode potentials repeatedly) and/or inactivation owing to exposure to H_2O_2 (Todorovic et al., 2015). In fact, we observe that electrode manipulation plays a major role in the loss of the catalytic performance. It is noteworthy that the ring Ag electrodes, used throughout this work, are specially designed for SERR spectroscopy, and are not optimized for multiple usage. Taking this into consideration, together with the good shelf-life of the wt and 29E4 based electrodes, we propose their use for the development of a disposable biosensor.

The selectivity of the wt and 29E4 PpDyP bioelectrodes was further tested in the presence of potential interfering substances: ascorbate,

Table 2

Analytical parameters of electrochemical H_2O_2 biosensors based on HRP. SWCNT – single walled carbon nanotubes; GC – glassy carbon; OANW – oleylamine-stabilized gold nanowires; C-Dots – carbon nanodots; LDHs – layered double hydroxides; 3-CPDS – 3-Carboxypropyldisulfide SAM; G – graphite electrode; Pan – polyaniline; MWCNTCOOH – carboxy-functionalized multiwalled carbon nanotube; CNT – Carbon nanotubes; AuNPs – gold nanoparticles; Chit – Chitosan; poly – polymerized; CESM – Carbonized chicken eggshell membrane; TH/SAME – thionine-modified SAM electrode; nano-Au – nano-scaled particulate gold; CCE – carbon ceramic electrode; GNP-TNT – gold nanoparticle dotted TiO_2 nanotubes; HIL – hydrophobic ionic liquid; PEGDGE – poly(ethyleneglycol) diglycidyl ether; $[Os(dmp)PVI]^{+/2+}$ – osmium redox polymer. All values refer to 3rd generation biosensors except for those marked with * which refer to 2nd generation (mediated) biosensors.

Bioelectrode	LOD (µM)	Linear Range (µM)	Response time (s)	Sensitivity ($A \cdot M^{-1} \cdot cm^{-2}$)	Reference
HRP/DNA-SWCNT/GC	0.3	0.6–1800	–	0.62	Zeng et al. (2009)
HRP-OANW/Au	5	20–500	–	0.031	Koposova et al. (2014)
HRP/C-Dots/LDHs/GC	0.04	0.1–23.1	–	0.47×10^{-3}	Wang et al. (2015)
HRP/3-CPDS/Au	–	100–1000	–	4.24×10^{-4}	Gaspar et al. (2001)
HRP/G	0.071	0.5–130	–	0.338	Gaspar et al. (2000)
HRP/Pan/MWCNTCOOH/Au	86	86–10000	2.9	0.195	Hua et al. (2011)
HRP/MWCNTCOOH/Au	26	26–8000	2.3	0.175	Hua et al. (2011)
Au/SAM/HRP/CNT	0.02	0.107–120	–	–	Kafi et al. (2018)
HRP/AuNPs	0.41	0.5–70	–	0.193	Narayanan and Slaughter (2019)
HRP/laponite/Chit/GC	5	29–1400	10	19.7×10^{-3}	Shan et al. (2010)
HRP/polyAuNPs/Au	1.5	5–1100	8	498×10^{-3}	Villalonga et al. (2011)
HRP/AuNPs/CESM/GC	0.3	10–2700	3	–	Zhang et al. (2015)
TH/HRP/SAME/Au*	40	40–100	–	2.5×10^{-3}	Ruan et al. (1998)
HRP/nano-Au/CCE/GC*	6.1	12.2–1100	8	0.29	Lei et al. (2004)
GNP-TNT/HIL/HRP/GC*	2.2	15–750	3	0.228	Liu et al. (2012)
HRP/PEGDGE/$[Os(dmp)PVI]^{+/2+}$/G*	0.3	1–500	3	0.297	Bollella et al. (2018)

Fig. 4. Stability of wt (gray) and 29E4 PpDyP/SAM/Ag (green) electrodes response to H_2O_2. Relative catalytic current response to 50 µM H_2O_2, during storage at 4 °C for 1 month (shelf-life) measured on a batch of electrodes prepared on the same day (n = 16). Inset: relative catalytic current measured using the same electrode (n = 4) during a 5 day period. (For interpretation of the references to color in this figure legend, the reader is referred to the Web version of this article.)

citrate, ethanol, sucrose, glucose and O_2, which are likely to be present in real samples. The respective responses were evaluated by a comparison of the catalytic current obtained upon addition of H_2O_2 (10 µM final concentration) in the presence or absence of 10 times higher concentration of hypothetical interfering substances. No interference is detected for the compounds tested (Table S2).

4. Conclusions

Reliable, fast, sensitive, selective and low-cost H_2O_2 sensors are highly sought after for numerous applications. To this end, continuous efforts are being made to explore i) novel biocatalysts with improved stability and catalytic performance, including plant peroxidases (e.g. HRP, tobacco peroxidase and new tropical plant peroxidases), CcP, chloroperoxidase, lactoperoxidase, etc. (Bollella and Gorton, 2018); ii) diverse electrode materials and coatings, which ensure high enzyme loading and efficient DET, such as polymers, nanostructures and recently reported quantum dots (Wang et al., 2015); and iii) simple and sensitive analytical methods for detection of the catalytic signal. To the best of our knowledge, we report here the first thorough characterization of a 3rd generation electrochemical biosensor for H_2O_2 detection based on DyP-type peroxidases with improved properties tailored by directed evolution. We evaluate the analytical performance of the wt PpDyP and three variants in solution and immobilized states and show that two biocatalysts are exceptionally well fit for the envisaged purpose. Both, wt and 29E4 PpDyPs represent excellent candidates for construction of H_2O_2 biosensors, as they show superior sensitivity and shorter response times compared to HRP based H_2O_2 biosensors reported so far in the literature (Shan et al., 2010; Villalonga et al., 2011; Zhang et al., 2015). They are stable for prolonged periods during storage and are insensitive to the presence of possible interference agents. This makes them remarkably suitable for development of biosensors in disposable, single-use configuration, based on e.g. silver screen-printed electrodes, for a variety of biological applications (Guo, 2016; Guo and Ma, 2017; Fu et al., 2019).

We highlight the importance of integrated, multidisciplinary approach to simultaneously evaluate the structure and catalytic properties of the enzymes in solution and immobilized state. We demonstrate that the catalytic parameters in solution are not indicative of the enzymes' electrocatalytic performance in the immobilized state, which is relevant for the development of the 3rd generation biosensors. A matrix of criteria was necessary to discriminate between the enzymes and allow for a prediction of their potential for the desired application. Surprisingly, preservation of the native structure upon enzyme immobilization, which can be determined by SERR spectroscopy and is the most common determinant for the success or failure of 3rd generation bioelectronics devices (Todorovic et al., 2006), has not provided any insights for differentiation between the wt and variant PpDyPs. The native structure is well preserved upon attachment of all studied enzymes to biocompatible metal supports and only their thorough kinetic and analytical characterization allowed for identification of the best performing biocatalyst. To that end, wt and 29E4 PpDyPs show subtle differences in H_2O_2 sensing, which makes them equally suitable for the foreseen application.

These enzymes can be further explored for bioelectrocatalysis of other DyP substrates, such as inert environmentally harmful dyes (e.g. phenolic and azo dyes) or lignin related compounds and their valorization, or further improved as H_2O_2 biosensors with higher accuracy and reproducibility for clinical or tissue engineering applications. As an additional evident advantage, PpDyP can be easily overexpressed in *E. coli* and manipulated to produce specific variants by rational design or directed evolution, which offers close to limitless opportunities for tailored applications employing immobilized PpDyP variants.

Declaration of competing interest

The authors declare that they have no known competing financial interests or personal relationships that could have appeared to influence the work reported in this paper.

CRediT authorship contribution statement

Catarina Barbosa: Investigation, Visualization, Validation. **Célia M. Silveira:** Methodology, Visualization, Supervision, Funding acquisition, Formal analysis. **Diogo Silva:** Investigation. **Vânia Brissos:** Investigation, Validation. **Peter Hildebrandt:** Resources, Writing - review & editing. **Lígia O. Martins:** Methodology, Resources, Supervision, Funding acquisition. **Smilja Todorovic:** Conceptualization, Supervision, Writing - review & editing, Funding acquisition.

Acknowledgements

Appendix A. Supplementary data

Supplementary data to this article can be found online at https://doi.org/10.1016/j.bios.2020.112055.

References

Bernad, S., Soulimane, T., Lecomte, S., 2004. J. Raman Spectrosc. 35, 47–54.
Bollella, P., Gorton, L., 2018. Curr. Opin. Electrochem. 10, 157–173.
Bollella, P., Medici, L., Tessema, M., Poloznikov, A.A., Hushpulian, D.M., Tishkov, V.I., Andreu, R., Leech, D., Megersa, N., Marcaccio, M., Gorton, L., Antiochia, R., 2018. Solid State Ionics 314, 178–186.
Brissos, V., Tavares, D., Sousa, A.C., Robalo, M.P., Martins, L.O., 2017. ACS Catal. 7, 3454–3465.
Colpa, D.I., Fraaije, M.W., van Bloois, E., 2014. J. Ind. Microbiol. Biotechnol. 41, 1–7.
Das, P., Das, M., Chinnadayyala, S.R., Singha, I.M., Goswami, P., 2016. Biosens. Bioelectron. 79, 386–397.
Forman, H.J., Bernardo, A., Davies, K.J.A., 2016. Arch. Biochem. Biophys. 603, 48–53.
Fu, Y., Yang, H., Guo, J., 2019. IEEE Trans. Ind. Inf. 15, 6389–6394.

Gaspar, S., Popescu, I.C., Gazaryan, I.G., Gerardo Bautista, A., Sakharov, I.Y., Mattiasson, B., Csöregi, E., 2000. Electrochim. Acta 46, 255–264.
Gaspar, S., Zimmermann, H., Gazaryan, I., Csöregi, E., Schuhmann, W., 2001. Electroanalysis 13, 284–288.
Guo, J., 2016. Anal. Chem. 88, 11986–11989.
Guo, J., Ma, X., 2017. Biosens. Bioelectron. 94, 415–419.
Hildebrandt, A.G., Roots, I., 1975. Arch. Biochem. Biophys. 171, 385–397.
Hua, M.-Y., Lin, Y.-C., Tsai, R.-Y., Chen, H.-C., Liu, Y.-C., 2011. Electrochim. Acta 56, 9488–9495.
Kafi, A.K.M., Naqshabandi, M., Yusoff, M.M., Crossley, M.J., 2018. Enzym. Microb. Technol. 113, 67–74.
Kanger, J.S., Otto, C., 2003. Appl. Spectrosc. 57, 1487–1493.
Kapetanaki, S., Chouchane, S., Girotto, S., Yu, S., Magliozzo, R.S., Schelvis, J.P.M., 2003. Biochemistry 42, 3835–3845.
Koposova, E., Liu, X., Kisner, A., Ermolenko, Y., Shumilova, G., Offenhausser, A., Mourzina, Y., 2014. Biosens. Bioelectron. 57, 54–58.
Lei, C.X., Hu, S.Q., Gao, N., Shen, G.L., Yu, R.Q., 2004. Bioelectrochemistry 65, 33–39.
Linde, D., Pogni, R., Cañellas, M., Lucas, F., Guallar, V., Baratto, M.C., Sinicropi, A., Sáez-Jiménez, V., Coscolín, C., Romero, A., Medrano, F.J., Ruiz-Dueñas, F.J., Martínez, A.T., 2015. Biochem. J. 466, 253–262.
Lippert, A.R., Van de Bittner, G.C., Chang, C.J., 2011. Acc. Chem. Res. 44, 793–804.
Liu, X., Feng, H., Zhang, J., Zhao, R., Liu, X., Wong, D.K.Y., 2012. Biosens. Bioelectron. 32, 188–194.
Ly, H.K., Sezer, M., Wisitruangsakul, N., Feng, J.J., Kranich, A., Millo, D., Weidinger, I.M., Zebger, I., Murgida, D.H., Hildebrandt, P., 2011. FEBS J. 278, 1382–1390.
Mendes, S., Brissos, V., Gabriel, A., Catarino, T., Turner, D.L., Todorovic, S., Martins, L.O., 2015a. Arch. Biochem. Biophys. 574, 99–107.
Mendes, S., Robalo, M.P., Martins, L.O., 2015b. Bacterial enzymes and multi-enzymatic systems for cleaning-up dyes from the environment. In: Singh, S.N. (Ed.), Microbial Degradation of Synthetic Dyes in Wastewaters. Springer International Publishing, Cham, pp. 27–55.
Monteiro, T., Almeida, M.G., 2019. Crit. Rev. Anal. Chem. 49, 44–66.
Munakata, H., Oyamatsu, D., Kuwabata, S., 2004. Langmuir 20, 10123–10128.
Murgida, D.H., Hildebrandt, P., 2001. J. Phys. Chem. B 105, 1578–1586.
Murgida, D.H., Hildebrandt, P., 2004. Acc. Chem. Res. 37, 854–861.
Narayanan, J.S., Slaughter, G., 2019. Bioelectrochemistry 128, 56–65.
Presnova, G., Grigorenko, V., Egorov, A., Ruzgas, T., Lindgren, A., Gorton, L., Börchers, T., 2000. Faraday Discuss 116, 281–289.
Rahmanpour, R., Rea, D., Jamshidi, S., Fulop, V., Bugg, T.D., 2016. Arch. Biochem. Biophys. 594, 54–60.
Roberts, J.N., Singh, R., Grigg, J.C., Murphy, M.E., Bugg, T.D., Eltis, L.D., 2011. Biochemistry 50, 5108–5119.
Ruan, C., Yang, F., Lei, C., Deng, J., 1998. Anal. Chem. 70, 1721–1725.
Santos, A., Mendes, S., Brissos, V., Martins, L.O., 2014. Appl. Microbiol. Biotechnol. 98, 2053–2065.
Sezer, M., Genebra, T., Mendes, S., Martins, L.O., Todorovic, S., 2012a. Soft Matter 8, 10314–10321.
Sezer, M., Millo, D., Weidinger, I.M., Zebger, I., Hildebrandt, P., 2012b. IUBMB Life 64, 455–464.
Sezer, M., Santos, A., Kielb, P., Pinto, T., Martins, L.O., Todorovic, S., 2013. Biochemistry 52, 3074–3084.
Shan, D., Li, Q.-B., Ding, S.-N., Xu, J.-Q., Cosnier, S., Xue, H.-G., 2010. Biosens. Bioelectron. 26, 536–541.
Singh, R., Eltis, L.D., 2015. Arch. Biochem. Biophys. 574, 56–65.
Singh, R., Grigg, J.C., Armstrong, Z., Murphy, M.E.P., Eltis, L.D., 2012. J. Biol. Chem. 287, 10623–10630.
Smulevich, G., Feis, A., Howes, B.D., 2005. Acc. Chem. Res. 38, 433–440.
Sugano, Y., 2009. Cell. Mol. Life Sci. 66, 1387–1403.
Todorovic, S., Hildebrandt, P., Martins, L.O., 2015. Phys. Chem. Chem. Phys. 17, 11954–11957.
Todorovic, S., Jung, C., Hildebrandt, P., Murgida, D.H., 2006. J. Biol. Inorg. Chem. 11, 119–127.
Todorovic, S., Rodrigues, M.L., Matos, D., Pereira, I.A.C., 2012. J. Phys. Chem. B 116, 5637–5643.
Todorovic, S., Verissimo, A., Wisitruangsakul, N., Zebger, I., Hildebrandt, P., Pereira, M.M., Teixeira, M., Murgida, D.H., 2008. J. Phys. Chem. B 112, 16952–16959.
van Bloois, E., Torres Pazmino, D.E., Winter, R.T., Fraaije, M.W., 2010. Appl. Microbiol. Biotechnol. 86, 1419–1430.
Villalonga, R., Díez, P., Yáñez-Sedeño, P., Pingarrón, J.M., 2011. Electrochim. Acta 56, 4672–4677.
Wackerbarth, H., Klar, U., Gunther, W., Hildebrandt, P., 1999. Appl. Spectrosc. 53, 283–291.
Wang, Y., Wang, Z., Rui, Y., Li, M., 2015. Biosens. Bioelectron. 64, 57–62.
Zeng, X., Li, X., Liu, X., Liu, Y., Luo, S., Kong, B., Yang, S., Wei, W., 2009. Biosens. Bioelectron. 25, 896–900.
Zhang, D., Zhao, H., Fan, Z., Li, M., Du, P., Liu, C., Li, Y., Li, H., Cao, H., 2015. PloS One 10 (6), e0130156.
Zhang, R., Chen, W., 2017. Biosens. Bioelectron. 89, 249–268.